XMM Flight Model Mirror effective area measurements

Y. Stockman, H. Hansen, Y. Houbrechts, J. Ph. Tock
CSL – University of Liège
B- 4031 Angleur, Belgium
email : ystockman@ulg.ac.be

D. de Chambure, Ph. Gondoin
ESA / ESTEC
PO BOX 299, 2200 AG Noordwijk, The Netherlands

ABSTRACT

The high throughput X-ray Spectroscopy Mission XMM is a "Cornerstone" project of the ESA Horizon 2000 Science Programme. The optical heart of this satellite consists in 3 Mirror Assemblies (MA). Each MA includes a Mirror Module (MM) containing 58 X-ray optical quality Mirror Shells (MS) and an X-ray baffle (XRB) which reduces straylight. Two of the three MAs are equipped with a Reflection Grating Assembly (RGA) for spectral analysis. Tests are performed in the CSL FOCALX facility. The goal of the presented tests is to evaluate the X-ray effective area of a MM. These tests are accomplished in a vertical configuration. An X-ray pencil beam is used for X-ray reflectivity measurements at Al, Au, Cu and Mo lines between 1.5 and 13 keV. A partial illumination collimated X-ray beam with a C continuous spectrum allows to measure the effective area of the MM over a 1.5 – 9 keV range.

This paper gives a short description of the tested specimens, and presents the test configuration in CSL Focal X facility. The paper focuses on a complete and original way to work out experimentally effective areas of an X-ray telescope. Analysis of the achieved results is carried out.

KEYWORDS :
X-ray optics and telescope, effective area, test facility, XMM

1. Introduction

The X-ray Multi-Mirror Mission (XMM)[1] is the second of the four "Cornerstone" projects in the ESA Long-Term Programme for Space Science "Horizon 2000". XMM is the largest scientific instrument ever built by ESA and will provide unprecedented abilities to the astronomical scientists for the study of high-energy phenomena. XMM's unique capability results in the combination of good imaging resolution, wide band spectral coverage and very high throughput.

The XMM satellite[2] includes 3 Mirror Assemblies (MA). Each MA consists of a Mirror Module (MM) containing 58 X-ray optical quality Mirror Shells (MS) and an X-ray baffle (XRB) to reduce the straylight. Two of the three MAs are equipped with a Reflection Grating Assembly (RGA) for spectral analysis.

Extensive testing have been carried out in the FOCALX test facility at the Centre Spatial de Liège (CSL)[3] in Belgium between 96-98 to verify the performance and to space qualify the 4 MMs without and with the XRB integrated. The performance of the XRB has also been checked[4] as well as the integration and the correct alignment of the RGA[5].

The XMM X-ray calibrations are performed at the Max Planck Institut (MPE)[6]. One of the main calibration requirement of the scientific community is an absolute measurement of the effective area. This one is defined as the product of the reflectivity times the geometrical section of the mirrors. It characterises the throughput of the telescope. Since no cosmic x-ray source can be used as in-orbit calibration standards, it is mandatory to perform calibration accurately on ground. The knowledge of the effective area should be between 2 – 3 percents in the 0.1 to 10 keV range, to allow the astronomers correct interpretation of the acquired data.

To achieve this high accuracy, numerous tests have been conducted at CSL and at MPE. Unfortunately none of these tests are fully representative of the in flight operation. Indeed, the full aperture X-ray tests at the MPE are compromised by the finite distance of the source. This configuration induces geometrical vignetting and higher incidence angle on the MS. Full aperture illumination tests at CSL with an infinite source distance are performed in the EUV[4]. A numerical model has been

developed[7,8] which simulates the reflection efficiency of the mirrors, and it geometry. These are the main parameters, which influence the effective area. Measurements were also performed at the MPE in the Panter test facility, using subapertures. This method reduces the beam divergence to 40 arcsec, but cover only a fraction of the XMM MM entrance plane. By rotating a variable aperture wheel it is possible to cover completely the MM entrance plane. Such configuration is close to the flight configuration, and the results can be regarded as absolute effective area calibration of the MM. However these tests have been done only at 1.5 and 8 keV.
In order to extend the energy coverage, an X-ray collimator with a C continuous source and a solid state detector in the MM focal plane were used at CSL. The advantage is to illuminate the MM with a parallel beam in the interesting energy range. Once again the set-up is quite representative of the flight configuration, but only a partial illumination is achieved. This means, that it is necessary, to scan, or to extrapolate, to the entire MM entrance plane.
This paper will first present an XMM MM, followed by the status of the knowledge of the effective area achieved on the XMM MM in terms of experimental results. In a second step, the presentation of the new experimental configuration used is exposed. A summary of the method followed to measure effective area and an analysis of the results is carried out.

2. Description of an XMM Mirror Module

The tested specimens are the XMM Flight Model Mirror Module[2,6], as shown in figure 1. This one is a grazing incidence telescope optimised to work in the 0.1 to 12 keV energy band with a focal length of 7.5 m and a spatial resolution of 16 arcsec or better. One Mirror Module contains 58-nested Wolter I telescope coaligned and cofocused. The effective width of the Mirror Shells aperture ranges from 1.5 mm for the smallest to 3 mm for the largest. The grazing incidence angle of the X-rays varies from 17 arcmin to 40 arcmin from the smallest one to the largest one respectively. All the Mirror Shells are interfaced to one spider at one end. This spider is interfaced to the Mirror Interface Structure providing the mechanical connection with the spacecraft platform. At 85 mm in front of this spider, an X-ray baffle[10] is mounted to reduce straylight from sources out of the FOV (Field Of View). The baffle consists of a series of "sieve plates", made out of circular strips. These plates are aligned in line with the front face of the mirrors, such that they block the single hyperbola reflection, without vigneting the two reflection rays.
All the Mirror Modules have been submitted to an acceptance and a calibration test programme. The goals of these tests[4] are to characterise the image quality of a flight configuration, to verify the stability of the optical performance after environmental tests (thermal cycling and vibration), and after the XRB integration. The X-ray calibration tests have been performed at the Panter MPE[6] facility.

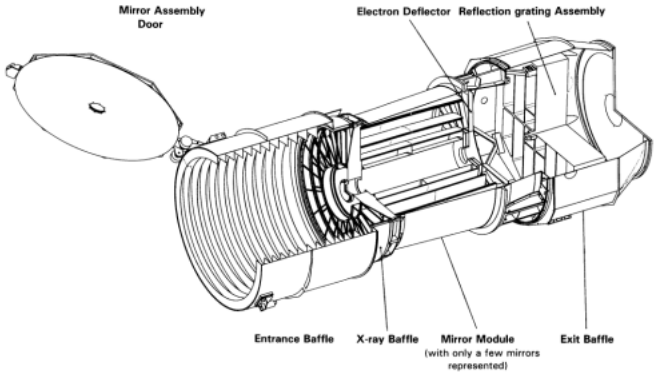

Focal length	7500 mm
Resolution Half Energy Width Full Width Half Max	 16 arcsec (0.1 - 12 keV) 8 arcsec (0.1 - 12 keV)
Effective area	1475 cm_ at 1.5 keV 580 cm_ at 8 keV
Reflective coating	Gold (250 nm)
Mirror diameter Outermost Innermost	 700 mm 306 mm
Axial parabola length	300 mm
Axial hyperbola length	300 mm
Mirror thickness	0.47 – 1.07 mm
Packing distance	1 – 5 mm
Numbers of mirrors	58
Mirror Module Mass	425 kg

Figure 1. **: Optical layout of an XMM MA and main requirements of a MM**

3. Status of effective area evaluation

3.1. CSL X-ray pencil beam tests

The first method used to measure the X-ray effective area is to analyse the reflectivity data achieved with the pencil beam channel[3]. This channel consists in two 0.3 mm-diameter pinholes separated by 7540 mm in front of a classical Electron Impact Point Source. The detector is a solid state detector. This set-up provides a 0.5 mm diameter X-ray pencil beam at entrance of the Mirror Shell with a divergence less than 30 arcsec. X-ray pencil beam tests are performed on all the MS before and after the XRB integration for all the MM FM's. The intensity measured at solid state level corresponds to the intensity of the beam reflected consecutively on the parabola and hyperbola section. This intensity is divided by the measured direct flux obtained once the MM is out of the beam. This computation is accomplished at 1.5, 2.1, 2.2, 8, 8.9, 9.7, 11.5 keV on all the MS. This provides a sample of reflectivity data (two reflections) over the spectral working range of XMM. Instead of plotting the reflectivity versus the MS number, it is better to present the reflectivity versus the incident angle. Since the pencil beam axis is parallel to the MM optical axis, the grazing angles are similar on the parabola and the hyperbola section and ranges from 17 arcmin on the smallest MS to 40 arcmin on the largest MS. The theoretical reflectivities are computed using these grazing angles and gold optical constants. Two sets of optical constants are used and compared, the first one is coming from "http://www-cxro.lbl.gov/optical_constants web site"(Henke-Gullikson), the other one is given in reference 11. The raw data is compared to these theoretical values calculated with the two sets of optical constants. For both cases the experimental data is lower than the predicted values.

To analyse the reflectivity measurement, it is necessary to correct the reflectivity loss due to scattering. This loss comes from the limited size of the detector (diameter 20 mm). Wing scattering measurements performed with the same X-ray pencil beam channel show that the scattering losses outside this diameter is 0.2 % at 1.5 keV and 6 % at 8 keV. Unfortunately no angle scattered measurements between these two energies are available. However, the missing intensity due to scattering is assumed to vary in a first approximation as a function of λ^2. This allows to correct the reflectivity measurements by the scattering loss for all the used wavelengths.
Comparison of the corrected data and the theoretical curves (figure 2.a) shows that the theoretical values are still higher. However, the use of the Zombeck optical constants[10] allows a better fit to the experimental data. To fit the reflectivity values using the Henke-Gullikson constants, two corrections have to be implemented. First, the introduction of a dust contamination. This provides simple vignetting and consequently a reduction of reflectivity. Second, modification of the gold coating density. The two figures 3 show the impact of the dust (3.a) and of lower gold density (3.b) on the theoretical curves. Adjusting these two parameters allows to get a fairly good fitting with the experimental data[7]. Correcting the experimental data by scattering and using the Zombeck optical constants allows also to achieve a correct fitting as shown in figure 2.b. The variations around the theoretical value are mainly explained by the micro-roughness difference of the MS.

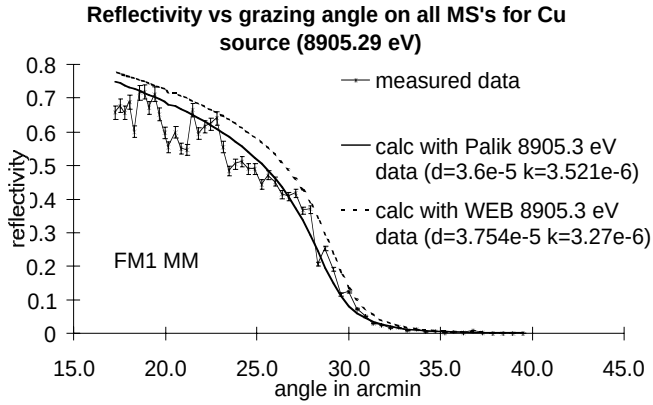

Figure 2.a : **Reflectivity measurements of MM with a Cu source 8.9 keV**

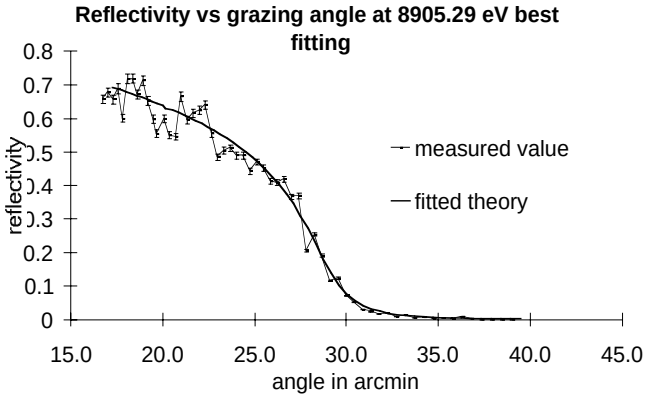

Figure 2.b : **Best fitting of the theoretical curve to the experimental data**

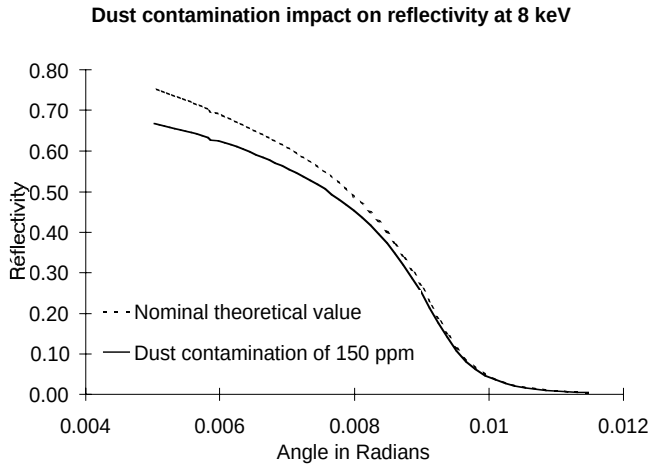

Figure 3.a : **Reflectivity modification due to a addition of dust on the optical surfaces**

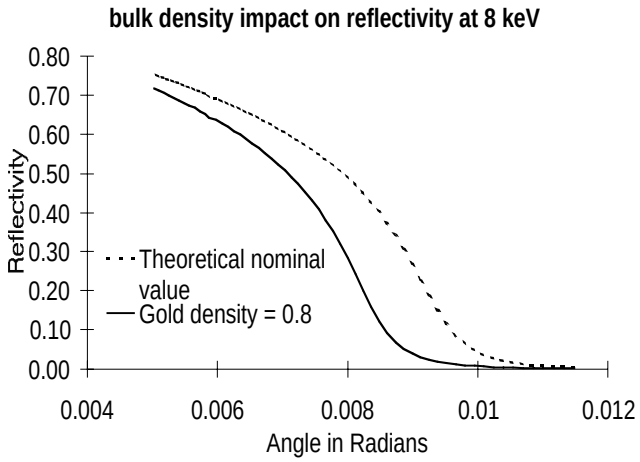

Figure 3.b : **Reflectivity modification due to a variation of the Gold density**

Using the reflectivity values corrected by the scattering, it is possible to evaluate the effective area of a MM, using the following formula:

$$Eff\_area = \sum_{i=1}^{58} R_i * Geom\_area_i$$

where R_i is the measured reflectivity (Parabola + hyperbola) and $Geom\_area_i$ is the designed geometrical area of the i^{th} MS taking into account the spider shadowing. This computation has been done for all the MM FM that will be integrated on the spacecraft and are presented in the comparison table in figure 6. These results are discussed in the preliminary conclusions on the effective area status.

3.2. XMM numerical models

The utilisation of the reflectivity data and the wing scattering measurements improves and verifies the XMM SCISIM[8] numerical model. The model takes into account the actual measured shape of the MS. It provides effective area curves versus energy for several source positions. These ones are used to compare the measured effective areas. For the analysis of the effective area measurements, a simplified model is built. This model uses the nominal optical parameters of the MSs, and the Henke-Gulikson optical constants (http://www-cxro.lbl.gov/optical_constants/). Comparison of the two models is shown in the figure 4. The simplified model done at CSL doesn't take into account the MS metrology data, neither the correction of reflectivity (as presented previously in 3.1). A simple multiplication factor (0.933) is applied to fit the SCISIM data in the 1 to 3 keV range. The fitting is worse at higher energy because the gold density has not been modified in CSL model. The SCISIM results are used in all the comparisons with the experimental data. The CSL model is only used to evaluate subaperture effective area experimental results (see §5.4).

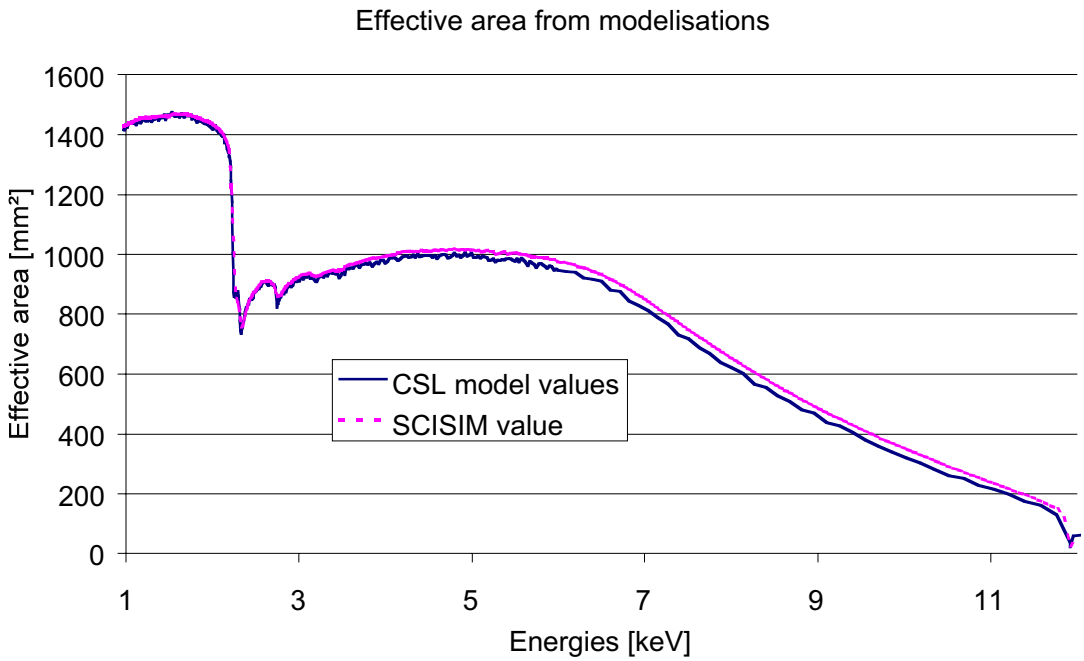

Figure 4: **Comparison of the two modelisations. For energies lower than 3 keV the fitting is fairly good between the two models. For higher energies the CSL model gives slightly lower values.**

3.3. Preliminary conclusions on the status of MM effective area measurements

Since the pencil beam measurements are local measurements (about 0.5 % of the total MM surface is sampled), several tests were conducted in the MPE Panter Facility at Neuried[6,12]. The experimental set-up consists in an X-ray source at 124 m in front of the MM. This configuration provides not an adequate situation. The measured effective area differences are 15-16 % lower than ideal values in the 0.3 – 6.4 keV energy band. The discrepancies can reach 20 – 30 % at higher energies. This is unacceptable. Moreover, once the XRB is integrated, this configuration cannot be used anymore. To overcome these difficulties, and to predict the effective area in representative operation conditions, a new test campaign was undertaken in the MPE Panter facility. Only a quarter of a sector is illuminated to simulate parallel beam illumination. The computed divergence was ≅ 40 arcsec in the worst case. The results obtained with this method give an absolute accuracy of 2 %[12].

The table in figure 5 summarises the results achieved with this MPE tests and the CSL reflectivity tests, compared to the expected theoretical value (using ideal coating reflectivity (Henke-Gullikson constant) and perfect geometry) and the SCISIM values.

CSL measurements, using the measured reflectivities corrected from scattering loss, are in good agreement with the one measured at MPE. At 1.5 keV the differences are lower than the announced absolute error of 2%. At 8 keV, the differences are larger for FM2 and FM3 but is still less than 4 %. For FM4 the figures are pretty close to each other.

The SCISIM simulation gives results close to the measured one, and show that it is necessary to modify the optical constant otherwise the differences rise 8 to 12 %. The MM FM1 numerical model is used for comparison, because it is presently the only one available.

Other energies were used to measure effective area at MPE and CSL. Figure 7 compares the measurements performed at MPE and CSL to the SCISIM values and shows predicted values close to the measured ones.

At the time the X-ray collimator tests were conducted, the only available absolute effective area measurements were at 1.5 and 8 keV. It was mandatory to get information of the effective area behaviour between these two energies. At the end of each test sequence, after completion of the mandatory optical tests, opportunity was taken to perform additional calibration test in the available time slot. The goal of these measurements is to characterise the Mirror Module (MM) effective area behaviour close to the Gold M absorption edge. Several alternatives can be followed. One method to evaluate the effective area is to measure the reflectivity in the 2 – 8 keV energy range on all the MS, and to compare the values to the expected ones. This has been done at 2.1 and 2.2 keV, the only available lines in this spectral region.

A second method, is to perform pencil beam reflectivity measurements using a C continuum source. This was tested on the smallest mirror shell (MS58). Unfortunately the signal was very low (poor accuracy) and the method is time consuming. To increase the signal, an X-ray collimated channel was used. The next paragraphs focus on this topic.

[cm]	*theory*	*SCISIM*	*measured*	*measured*	*measured*	*measured*	*measured*	*measured*
energy	*effective*	*effective*	*MPE*	*CSL*	*MPE*	*CSL*	*MPE*	*CSL*
keV	*area*	*area*						
	perfect	FM1	**FM2**	**FM2**	**FM3**	**FM3**	**FM4**	**FM4**
1.50	1559.7	1466	1433	1416	1445	1425	1403	1417
8.00	686	611	618.3	595	599.8	578	593	596

Figure 5 **: Effective area results for MM FM's**

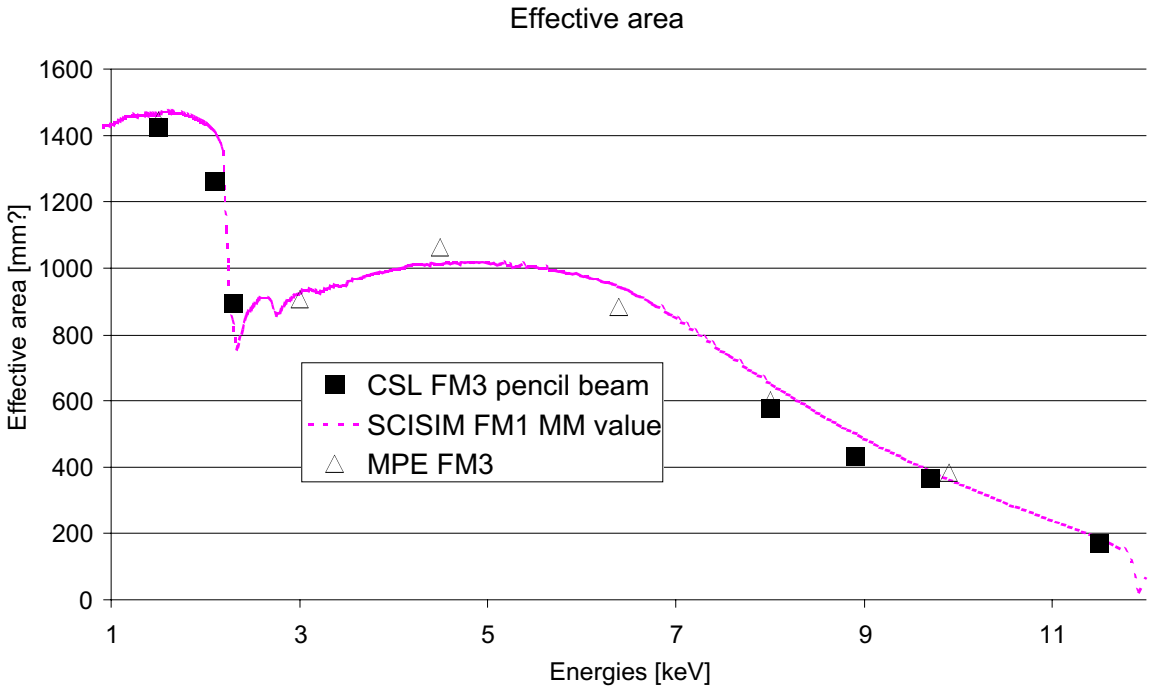

Figure 6 **: Comparison of the MPE and CSL measured effective area with respect to the SCISIM predicted values.**

4. X-ray collimator optical configuration

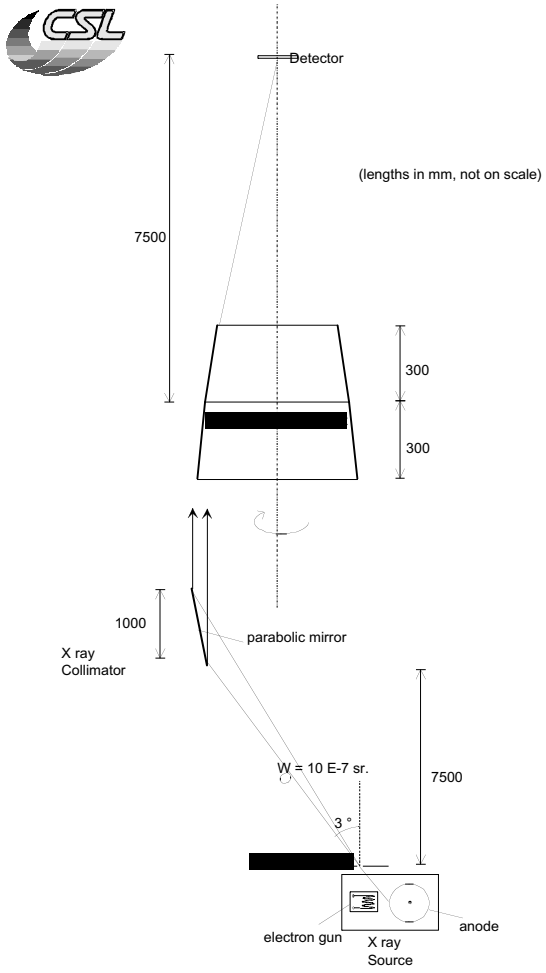

Figure 7 : **X-ray collimator channel general layout**

The optical configuration of this channel was already largely presented in previous papers[3]. Only a summary will be presented hereafter. A schematic view of this channel is shown in figure 7.

The source consists in a classical X-ray electron impact point source providing spectral lines between 1 and 15 keV of Al, Cu, Au, Mo when utilised as targets and a continuum when C anode is used. In front of this source a 100 µm diameter pinhole is placed. This one is located at the focal point of an off-axis parabola mirror which has a length of 1.2 m and a width of 80 mm. Due to the grazing angle on the mirror the effective aperture has a curved shape (see figure 8.g) of 80 * 8 mm_. The beam is restricted to 50 * 8 mm_ by a baffle to avoid the direct beam from the source to the MM and to use the high quality central part of the mirror. Between the pinhole and the mirror a filter wheel is integrated with thin metallic filter to eliminate the visible spectrum of the X-ray source. The collimated beam is focalised on a detector by the tested telescope. The detector is a front side illuminated CCD working in counting mode or a solid state detector. The advantage of the CCD is to provide spatial resolution, while the solid state detector gives the spectral resolution. These two detectors give the opportunity to use different ways to measure effective areas. All the optical parts are mounted on a rigid optical bench, mechanically decoupled from the ground vibrations. A small solid state diode is used, for monitoring purposes, just after the collimated beam.

4.1. Verification of the alignment

The system has been aligned[13] at atmospheric conditions using the focal point image of the off-axis parabolic mirror when illuminated by a perfect vertical collimated beam. The later one comes out a Zygo interferometer and is aligned vertically with the help of a liquid mirror. The alignment method of the off axis parabola is presented in ref 13. Once under vacuum, the only way to evaluate the correct alignment is to record the flat field provided by the channel. Simulations (see figures 8) show that this diagnostic tool is unsensitive in focus but sensitive in lateral displacement of the pinhole or tilts of the off axis parabolic mirror. Having the expected shape assumes that the collimator is correctly aligned with an accuracy of 1 mm at pinhole level (about 40 arcsec). However, due to the stiffness of the optical bench a displacement of 1 mm is not expected. Figure 8.g. presents an experimental X-ray collimator flat field, composed of a mosaic of 4 EUV CCD images. The flat field image presents some vertical strips. It is possible to make a correlation between these strips and the axial slope error of the mirror. Fortunately, these strips are perpendicular to the MS section, so that their impacts are minor.

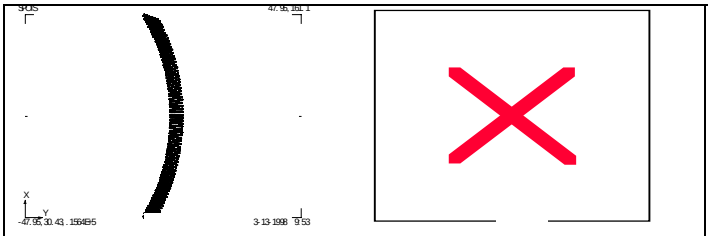

Fig 8.a and 8.b : Displacements normal to the parabolic surface change the length (from 98.9 to 66.5 mm) and the width (from 5.4 to 11.2 mm) of the collimated beam.

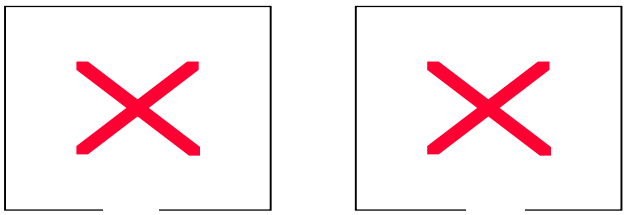

Fig. 8.c and 8.d : Displacement tangential to the parabolic surface doesn't change length, but modify the shape.

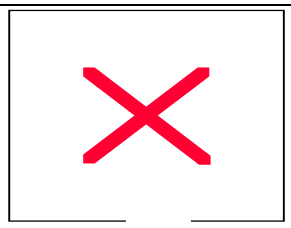

Figure 8.e and 8.f :

Impact of a 10 mm defocus. The length and the width change slightly from 79.7 mm to 80.2 mm and from 8.9 mm to 9 mm respectively.

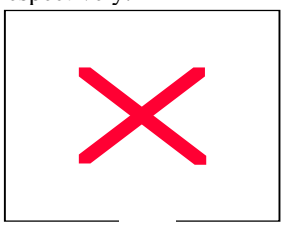

Figure 8.e : Experimental flat field

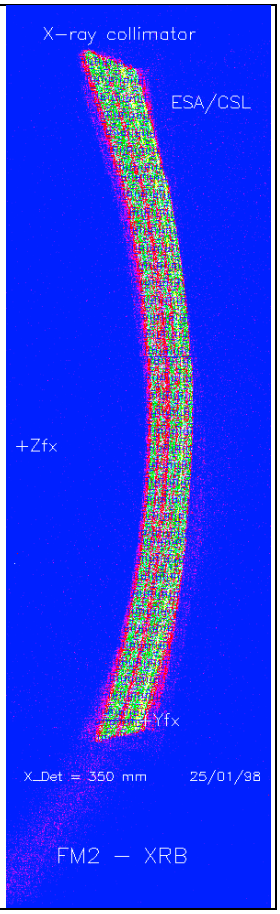

Figure 8 : **Influence of the source position on the shape of the collimated beam. To show the effect, a +/- 5 mm lateral displacements, and a +/- 10 mm in focus of the pinhole has been simulated.**

5. Effective area measurement with X-ray collimated beam

5.1. Principle

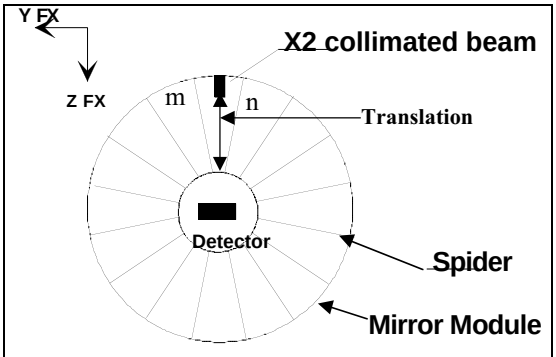

Figure 9 : **Axis definition and measuring set-up**

In order to measure effective area with the collimated beam, the detector is placed in the direct flux to measure the incident flux. The spatial homogeneity of the flux can be controlled with the CCD, the spectral homogeneity with the solid state detector. The alignment of the MM in front of the collimated beam is performed first by translating the MM laterally along Y_{FX} to determine the position of the two MM spiders (m,n). The MM can then be positioned in the middle of the sector. The second step consists in translating the MM in the Z_{FX} direction to determine the edge of the inner MS. Tests using the X-ray CCD have been reported previously[3] and showed that the method is promising. Differences between expected and measured effective area were lower than 2% at 1.5 keV on an inner ring. However, this method is limited to spectral line sources.

The new proposed method replaces the CCD detector by the solid state detector and the line source by a C continuous source. This setting allows to evaluate the effective area over a large spectral range. To simplify the procedure the MM doesn't rotate during the acquisition. Azimuthal distribution measurements performed in EUV at CSL and in X-ray at Panter show that the RMS throughput variation between each sector is around one percent.

5.2. Source setting

The source setting (voltage and intensity) is optimised in direct flux and in reflected flux over the first stack of MSs. This first stack corresponds to the smallest MSs and will provide the higher integrated reflected signal. For both situations (direct and reflected flux) the source voltage and intensity are set in such a way that the count rate at Canberra detector is lower than 1000 counts/s to ensure a negligible pile-up rate. This is possible, because the intensity of the direct beam has approximately the same amplitude as the reflected beam at detector level. Indeed, the solid state detector collects only a part (78 %) of the direct beam. The reflected beam is attenuated by two reflections (80 % to a few % depending of the MS stack and the energy). The dynamic range of the detector is only used for reflectivity. For source stability purposes, the intensity must be higher than 2 mA. If not, filters are added. During each acquisition the anode current and voltage are recorded every 20 s.

5.3. Data acquisition

Data acquisition sequence consists in :

1. Acquisition of a direct flux during one hour
2. Acquisition of a reflected flux on the first stack of MSs (small size) during one hour
3. Acquisition of a reflected flux on the second stack of MSs (medium size) during one hour
4. Acquisition of a direct flux during one hour
5. Acquisition of a reflected flux on the third stack of MSs (mid-large size) during one hour
6. Acquisition of a reflected flux on the fourth stack of MSs (large size) during one hour
7. Acquisition of a direct flux during one hour

One set of measurement takes about 10 hours (setting + 7 hours exposure time + displacements).

5.4. Data reduction

The incident flux is the average of the 3 direct flux measurements. It is normalised to the Canberra effective area taking into account the diameter, the Be mesh and direct flux size (8 * 50 mm_). The reflected flux is weighted by the number of X-ray collimator areas needed to cover the concerned MSs stack diameter. This means that the first reflected intensity is taken into account 137.5 times (176.7, 216 and 255.3 for the three next stacks respectively). 10 % is removed to take into account the MM spider shadowing. The Canberra detector energy scale has been calibrated by data acquired with the pencil beam and the direct collimated beam with the available spectral lines. To avoid the impact of possible source variations, the measured flux is divided by the average anode intensity of the source during the acquisition. The discrepancies with respect to the MM FM1 simulated values are small. To achieve a better fitting to the simulated value, the experimental data have to be multiplied by 1.04. This correcting factor is explained by the approximations performed at several stages of the analysis. One simple example is the use of the collimated banana shape, instead of a trapezoidal one. This means that several MS effective areas are taken into account more than other parts of the MM.

Further analyses using the CSL simplified model are performed to increase the confidence on the measurement. A first analysis is to compare the subaperture data with respect to the expected one. Using the collimated beam geometry and the MSs dimensions, the effective area is divided in 4 sub-areas corresponding to the 4 stacks of MSs illuminated. This effective area curves are then compared to the measured ones. This allows to determine bad measurements inside the 4 acquisitions. An example of this analysis is presented in the figures 10. These results are typical results i.e. the spectral behaviour of the subaperture effective area is the same for all the measurements performed up to now.

It is possible to introduce in our simple model various incidence angle, and to optimise the fitting with the experimental data. From the alignment setting it can be observed that the best alignment following Y_Det for the direct beam and the reflected beam differs by 3 500 µm. This corresponds to a tilt of 100 arcsec. The impact of this tilt on the effective area is low for such angles. Actually there is no impact for energies lower than 3 keV.

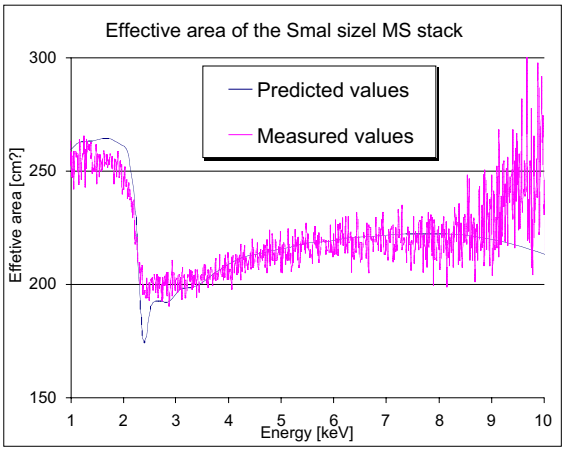

Figure 10.a : The general behaviour on the smallest MSs is that for energies higher than 8.5 keV the effective area takes off from the simulated curve. At 10 keV, the K edge of the Ge starts to become an influence. This is not observed for the other subaperture, because for these the signal is low.

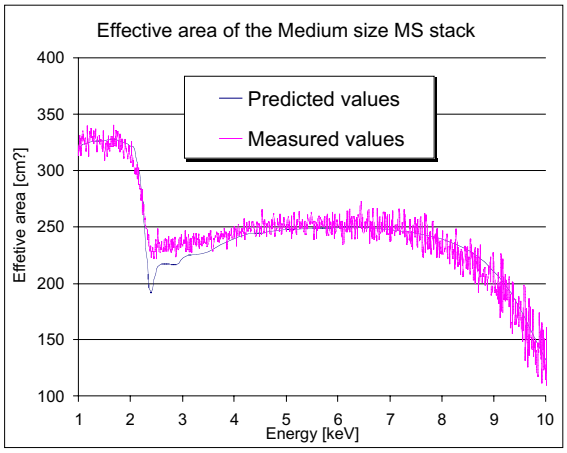

Figure 10.b : For the small mid MSs the fitting is usually correct. Due to the limited spectral resolution of the Solid State Detector the measurements splits from the modelled curve in the Gold M absorption edge region.

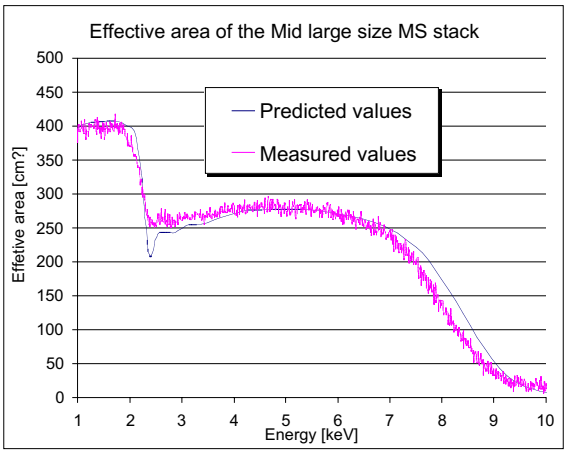

Figure 10.c : For the mid large MS stack, the same comments as for figure 10.b are valid, but the fitting between the two curves is worst.

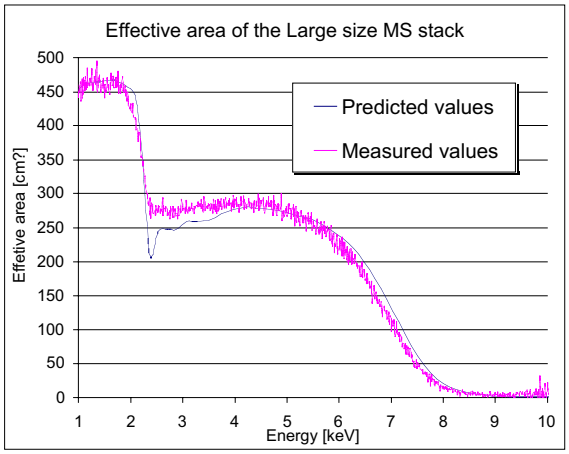

Figure 10.d : For the large MSs the effective area is always too low at low energies, which is also the case for the small MSs (figure 10.a), but also at energies higher than 4 keV.

Since the evaluation of the number of time (n) required to cover the MM entrance plane is a rough evaluation, an optimisation is performed on these numbers. The method is to perform a best fitting of the experimental curve to the theoretical one using the number that is necessary to multiply each stack of MSs (n factors). Making this operation a good fitting can be achieved, but the "n" numbers are completely inappropriate. Moreover the n parameters are computed to decrease the impact of the stacks having too large effective area at higher energies (small MS) and to increase the contribution of the stacks having higher effective area at lower energies.

5.5. Results of these analysis

All the data is available to perform a direct absolute effective area measurement. However due to the simplicity of the measurements and the non optimised set-up, the results can not be used as an absolute calibration. They are exploited to confirm that the effective area follows the expected behaviour between 1.5 – 9 keV energy range. The deviation between the SCISIM model and the measurements performed with the X-ray collimator is presented in figure 11. The differences are less than 2 % for energies higher than 4 keV. Close to the Gold absorption edge, some absorption edges are not recorded

and provides discrepancies up to 4 %, because of the low spectral band resolution of the detector. The measurement noise is evaluated to be around 1%.

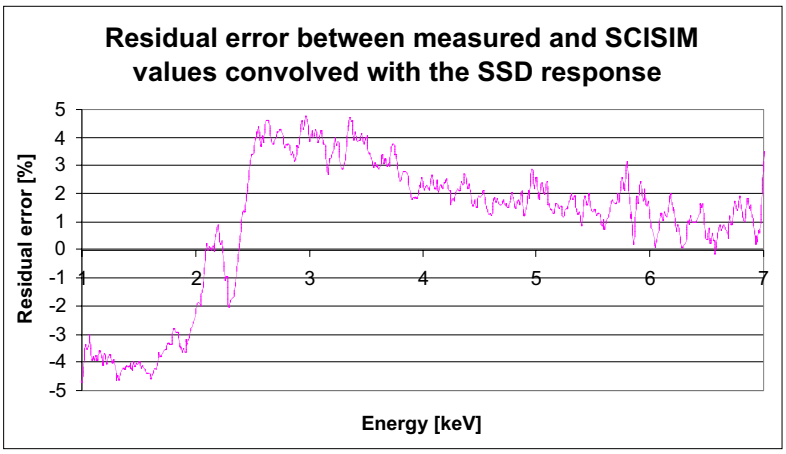

Figure 11 : **Residual error between Measured and SCISIM values. These last one are convolved with the spectral response of the solid state detector determined by line spectra**

The "plateau" before the Gold M absorption edge, is lower than the expected value. This effect is partially explained by the noisy response of the detector in this range. Attempts to decrease these residual errors by introducing tilts or changing the number to multiply by arbitrary constant, reduces this residual error (less than 1 %). Unfortunately these new numbers have no real physical meaning. The incoming beam is spectrally homogeneous, but not spatially (see figure 8.e). However as already mentioned the inhomogenities are perpendicular to the MS, and shouldn't have a high impact on the measurement accuracy.

6. Conclusions

Several methods used at CSL in the frame of XMM project to measure effective area have been presented. The results of each of these methods are summarised in figure 6 and 12 and are compared to predicted values or measurements performed at MPE. Each of the method has its own qualities and limitations, but leads to very consistent results.
The simple method using the reflectivity data corrected by scattering loss provides quite good results. Unfortunately, the method is not considered as reliable, because only a small part of the MM is sampled. Other cross calibrations are required. The absolute values measured with the pencil beam at CSL are confirmed by the MPE X-ray calibration test (see figure 5 and 6).

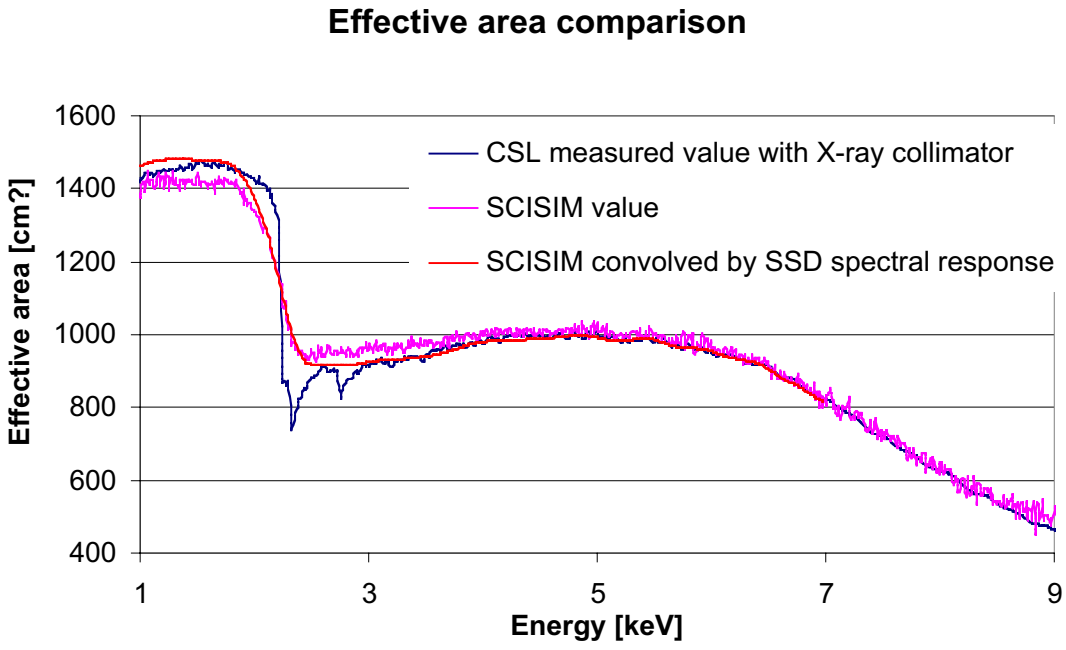

Figure 12 : **Comparison curves between numerical model and measurements**

Since the effective area was known at only two energies (1.5 and 8 keV), a new and original method to measure effective area for X-ray telescopes using an X-ray collimator has been developed. The method looks quite promising, since these first measurements give results close to the other experimental results and close to the expected one. In the worst cases the deviations are of 4 %. To increase the quality of this new measurement method, a trapezoidal mask should be integrated to achieve a better coverage of the MM entrance plane. The second improvement is in the procedure. During the acquisition of the reflected flux, the MM should be rotated. This would give the method independent of the azimuthal homogeneity of the MM. Using a solid state with a better spectral resolution would allow better results in the Gold M edge absorption spectral region.
If only the relative effective area is required, the results give valuable information about the behaviour of the effective area over a large part of XMM energy range (1.5 to 9 keV). With the present set-up and method it is possible to measure the absolute value of the effective area of a MM. The presently measurement accuracy is estimated around 4 %. This one can be reduced to 1 or 2 %, by implementing the improvements mentioned above.

Acknowledgements

We are grateful to all our colleagues who worked days and nights to perform the XMM MM testing.
We acknowledge the support of ESA XMM project team for the fruitful relations and collaborations.
The vertical facility at CSL was funded by ESA XMM project under the contract number 9939/92/NL/PP.
The XMM FM MM mirrors were replicated and integrated by MEDIA LARIO under ESA contract number 0545/93/NL/RE.

References

1. D. de Chambure, R. Lainé, K. van Katwijk, J. van Casteren & P. Glaude, “Producing the X-Ray Mirrors for ESA’s XMM Spacecraft”, ESA bulletin 89, February 1997.
2. R. Lainé, D. de Chambure, D. Kampf, G. Grisoni, “Results of thin X-ray mirror technology for ESA XMM Mission”, 48th IAF Congress, Torino, Italy, 1997.
3. J. Ph. Tock, J-P. Collette, Y. Stockman, “Calibration and upgrades of the XMM vertical EUV/X test facility: FOCALX”, SPIE 3114, pg 554, San Diego 1997.
4. Y. Stockman, I. Domken, H. Hansen, J.Ph. Tock, D. de Chambure, Ph. Gondoin, “XMM Flight Mirror Modules environmental and optical testing”, SPIE 3444 ,pg 302-312, San Diego 1998
5. Y. Stockman, I. Domken, H. Hansen, J.Ph. Tock, T.A. Decker, A. Rasmussen, T. den Boggende, J.W. den Herder, G. Bagnasco, D. de Chambure, C. Erd, Ph. Gondoin, “XMM Flight Mirror Module with Reflection Grating Assembly and X-ray baffle testing”, SPIE 3445 , San Diego 1998.
6. R. Egger, B. Aschenbach, H. Brauninger, W. Burkert, K. Molthagen, A. Oppitz, “Complementary X-ray calibration of the XMM mirror module FM3 at the Panter test facility”, XMM-TS-PA076/980515, Neuried, 1998.
7. Ph. Gondoin, M. Deijeysbergen, K. van Katwijk, D. Lumb, A.J. Peacock, “Simulation of the XMM performance based on metrology data”, SPIE 2808, pg 379-388, Denver, 1996
8. Ph. Gondoin, B. Aschenbach, M. Deijeysbergen, R. Egger, F. Jansen, Y. Stockman, J.P.Tock, “Calibration of the first XMM Flight Mirror Module II – Effective area”, SPIE 3444, pg 290, San Diego 1998.
9. D. de Chambure, R. Lainé, K. van Katwijk, “The X-Ray telescope for ESA XMM Spacecraft”, SPIE 3444 , San Diego 1998
10. D. de Chambure, R. Lainé, K. van Katwijk, J.P. Tock, I. Domken, Y. Stockman, M. Leonard, H. Hansen, W. Ruehe, E. Hoelzle, Y. Gutierrez, M. Domingo, “X-ray baffle of the XMM telescope : development and results” ,These proceedings, Berlin 99
11. E. Palik, “Handbook of Optical Constants of Solids”, Academic press, 1985.
12. R. Egger, B. Aschenbach, H. Brauninger, W. Burkert, T. Döhring, A. Oppitz, “X-ray calibration of the XMM mirror module FM3 at the Panter test facility”, XMM-TS-PA070/980115, Neuried, 1998
13. J-P. Collette, Y. Stockman, J Ph. Tock, " Performance of XMM optical vertical facility", SPIE 2808, pg350-361, Denver 1996.